Dalton Transactions

Mapping the Influence of Ligand Electronics on the Spectroscopic and 1O2 Sensitization Characteristics of Pd(II) Biladiene Complexes Bearing Phenyl-Alkynyl Groups at the 2- and 18-Positions

Journal:	*Dalton Transactions*
Manuscript ID	DT-ART-03-2023-000691.R1
Article Type:	Paper
Date Submitted by the Author:	06-Apr-2023
Complete List of Authors:	Martin, Maxwell; University of Delaware, Pham, Trong-Nhan; University of Delaware, Chemistry & Biochemistry Ward, Kaytlin; University of Delaware, Department of Chemistry & Biochemistry Rice, Anthony; University of Delaware, Department of Chemistry and Biochemistry Hertler, Phoebe; University of Delaware, Department of Chemistry & Biochemistry Yap, Glenn P A; University of Delaware, Gilmartin, Philip; University of Delaware, Department of Chemistry and Biochemistry Rosenthal, Joel; University of Delaware, Department of Chemistry and Biochemistry

Mapping the Influence of Ligand Electronics on the Spectroscopic and $^1O_2$ Sensitization Characteristics of Pd(II) Biladiene Complexes Bearing Phenyl-Alkynyl Groups at the 2- and 18-Postions

Maxwell I. Martin, Trong–Nhan Pham, Kaytlin N. Ward, Anthony T. Rice, Phoebe R. Hertler, Glenn P. A. Yap, Philip H. Gilmartin and Joel Rosenthal*

Department of Chemistry and Biochemistry, University of Delaware, Newark, DE, 19716

ABSTRACT:

Photodynamic therapy (PDT) is a promising treatment for certain cancers that proceeds via sensitization of ground state $^3O_2$ to generate reactive $^1O_2$. Classic macrocyclic tetrapyrrole ligand scaffolds, such as porphyrins and phthalocyanines, have been studied in detail for their $^1O_2$ photosensitization capabilities. Despite their compelling photophysics, these systems have been limited in PDT applications because of adverse biological side effects. Conversely, the development of *non-traditional* oligotetrapyrrole ligands metalated with palladium (**Pd[DMBil1]**) have established new candidates for PDT that display excellent biocompatibility. Herein, the synthesis, electrochemical, and photophysical characterization of a new family of 2,18-bis(phenylalkynyl)-substituted Pd^{II} 10,10-dimethyl-5,15-bis(pentafluorophenyl)-biladiene (**Pd[DMBil2–R]**) complexes is presented. These second generation biladienes feature extended conjugation relative to previously characterized Pd^{II} biladiene scaffolds (**Pd[DMBil1]**). We show that these new derivatives can be prepared in good yield and, that the electronic nature of the phenylalkynyl appendages dramatically influence the Pd^{II} biladiene photophysics. Extending the conjugation of the **Pd[DMBil1]** core through installation of phenylacetylene resulted in a ~75 nm red-shift of the biladiene absorption spectrum into the phototherapeutic window (600-900 nm), while maintaining the Pd^{II} biladiene's steady-state spectroscopic $^1O_2$ sensitization characteristics. Varying the electronics of the phenylalkyne groups via installation of electric donating or withdrawing groups dramatically influences the steady-state spectroscopic and photophysical properties of the resulting **Pd[DMBil2–R]** family of complexes. The most electron rich variants (**Pd[DMBil2–N(CH_3)$_2$]**) can absorb light as far red as ~700 nm but suffer from significantly reduced ability to sensitize formation of $^1O_2$. By contrast, **Pd[DMBil2–R]** derivatives bearing electron withdrawing functionalities (**Pd[DMBil2–CN]** and **Pd[DMBil2–CF_3]**) display $^1O_2$ quantum yields above 90%. The collection of results we report are suggest that excited state charge transfer from more electron-rich phenyl-alkyne appendages to the electron deficient biladiene core circumvents triplet sensitization. The spectral and redox properties, as well as the triplet sensitization efficiency of each **Pd[DMBil2–R]** derivative is considered in relation to the Hammett value (σ_p) for each biladiene's R-group. More broadly, the results reported in this study clearly demonstrate that biladiene redox properties, spectral properties, and photophysics can be perturbed greatly by relatively minor alterations to biladiene structure.

INTRODUCTION:

Photodynamic therapy (PDT) is a promising alternative treatment for certain types of cancers.[1] PDT is currently employed for cancers of the skin, bladder, and breast, as well as other dermatological conditions.[2–4] PDT works via administration of a photosensitizer drug that, upon irradiation with light, can energize to a triplet excited state. For Type II PDT, the excited photoagent sensitizes the formation of $^1O_2$, which is a potent oxidant of organic and biological matter. Phototriggered oxidative cell damage can result in either apoptotic or necrotic cell death and tumor ablation.[5–7] An ideal photosensitizer absorbs light in the phototherapeutic window (600-900 nm) so that the light can deeply penetrate epidermal tissues.[1] This mechanism for treatment highlights the promise of PDT as a localizable and efficient treatment, without the side-effects of surgical tumor removal or traditional chemotherapeutics.[8,9]

Most PDT photosensitizers fall into three principal families: BODIPY dyes,[10,11] Ru(II) polypyridyls,[12–14] and tetrapyrroles.[15,16] The tetrapyrrole family of photosensitizers, including porphyrins, chlorins, bacteriochlorins, and corroles, have been rigorously studied as PDT candidates (Figure 1a). Photofrin, which is a mixture of porphyrin oligomers, was the first clinically approved photosensitizer for PDT, and is still one of the most widely used in PDT treatment.[17] However, drawbacks of Photofrin include relatively weak absorption in the phototherapeutic window (λ_{max} = 630 nm, ε = 3,000 M^{-1} cm^{-1}), as well as patient's displaying high skin photosensitivity for multiple weeks post-procedure due to the photodrug clearing very slowly from epithelial tissues.[17,18] Following the translation of Photofrin to the clinic, new generations of tetrapyrrole-based

photosensitizers have been developed in efforts to improve light absorption and singlet oxygen generation, while minimizing patient side effects.

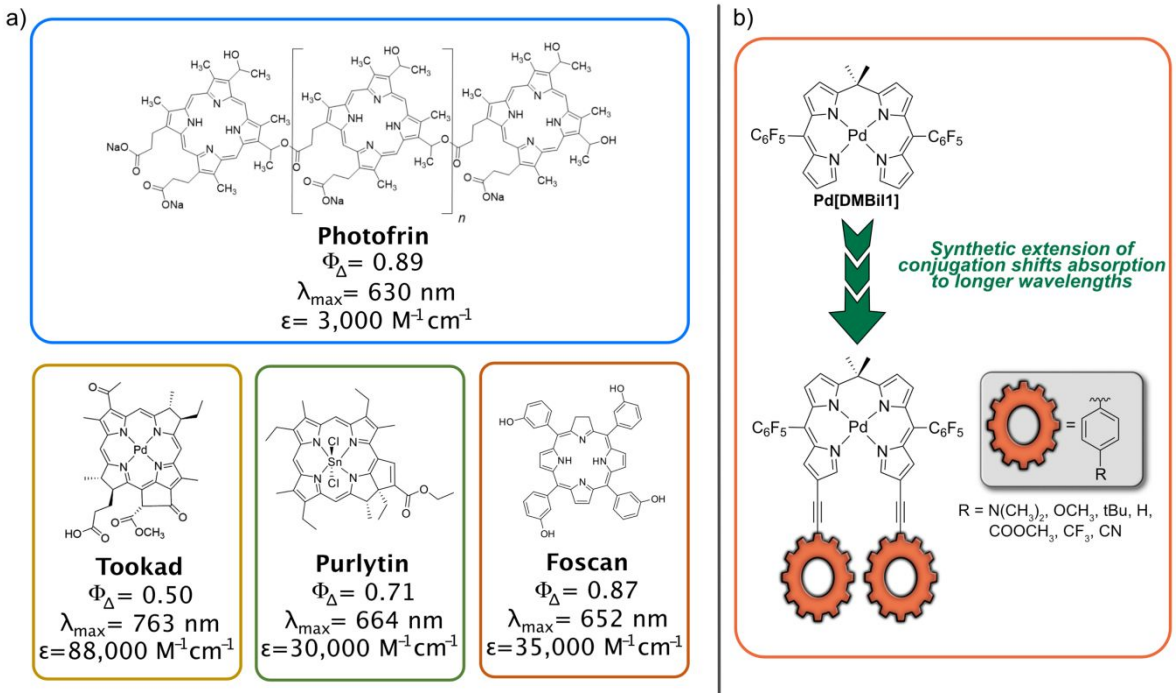

Figure 1: Various tetrapyrrole-based photosensitizers.

Two distinct synthetic approaches have been adapted to establish new tetrapyrrole-based photoagents for PDT. The above mentioned classes of tetrapyrroles possess only *sp*^{2}-hybridized atoms at the *meso*-positions that link the pyrrole units (*i.e.*, traditional tetrapyrroles are aromatic). Prior efforts have shown that substituting the *meso*-positions, can have a pronounced effect on the compound's photophysics and $^1O_2$ sensitization characteristics. Such is the case for Foscan (see Figure 1a), which bears *meso*-phenol functionalities on a chlorin backbone. This photosensitizer has been used in the treatment of various cancers, but suffers from slow clearance from physiological tissue.[19] A complementary strategy has entailed coordination of second row (or heavier) metal centers, such as palladium within the tetrapyrrole to promote more efficient $^1O_2$ sensitization through the heavy atom effect.[20–22] Examples of such agents include the

Pd(II) bacteriopheophorbide known as Tookad (see Figure 1a), which has been tested for PDT treatments of bladder[23] and prostate cancers.[24] Similarly, the Sn(IV) purpurin known as Purlytin (see Figure 1a) has been evaluated for the treatment of breast cancer, although it suffers from high dark toxicity and patient photosensitivity.[25]

Given that all aromatic tetrapyrrole-based agents for PDT have shortcomings that limit their clinical use, efforts have been focused on establishing new classes of *non-aromatic* tetrapyrroles that contain an sp^3-hybridized carbon-center at one of the *meso*-positions. Examples of non-aromatic tetrapyrrole scaffolds that support intriguing photophysical properties include phlorins[26–30], isocorroles[31–35], porphyrinogens[36–39], and biladienes,[40–44] some of which have shown potential to sensitize the formation of $^1O_2$. Prior work from our laboratory has established non-aromatic Pd(II) oligotetrapyrroles as potential PDT agents. More specifically, Pd(II) 10,10-dimethylbiladiene (**Pd[DMBil1]**), is comprised of an oligotetrapyrrole scaffold bearing a geminally disubstituted sp^3-hybridized *meso*-carbon that is coordinated to Pd(II). **Pd[DMBil1]** efficiently sensitizes $^1O_2$ with quantum yields of Φ_Δ = 54 % upon irradiation at 500 nm.[22] Upon coupling to a short PEG chain, the resulting water-soluble **Pd[DMBil1]–PEG$_{750}$** efficiently generates $^1O_2$ under biological conditions and displayed an exceptionally high phototoxicity index (PI > 5000) and efficacious treatment of MB-MDA-21 triple negative breast cancer cells.[45] The **Pd[DMBil1]** platform has also been considered for tandem photodynamic and photothermal therapies.[46,47] However, **Pd[DMBil1]–PEG$_{750}$** does not absorb deeply into the phototherapeutic window (λ_{max} = 580 nm), which has spurred our efforts to attenuate the biladiene electronics and push its light-harvesting ability into the phototherapeutic window (600-900 nm).[45]

There is a body of prior work by the tetrapyrrole community demonstrating that bathochromic shifting of absorption profiles can be realized by decreasing the HOMO-LUMO energy gap via extension of the π-conjugation of the tetrapyrrole and/or addition of electronically distinct functional groups on the molecule's periphery. This strategy has been successfully utilized to alter the absorbance profiles of porphyrins, phthalocyanines, and other organic chromophores for applications that include PDT and solar light harvesting.[48–52] Extending the π-conjugation system of chromophores can result in contraction of a tetrapyrrole's HOMO-LUMO gap by directly increasing the energy of the π-HOMO and decreasing the π*-LUMO.[53] For example, prior work has shown that installation of ethynyl functionalities off the *meso*- or β-positions of porphyrins extends the π-conjugation of such systems and significantly perturbs the tetrapyrrole's optical properties.[54–59] Addition of electron donating or withdrawing groups can also alter the HOMO or LUMO energy levels with respect to the parent unsubstituted compound.[60] We rationalized that combining both these strategies to attenuate the absorption properties of the parent **Pd[DMBil1]** would yield new biladiene constructs with absorption profiles better suited for use as PDT agents *in vivo*.[50,61–65]

Prior work has revealed that the **Pd[DMBil1]** scaffold can be functionalized via bromination at the 2- and 18- β-carbon positions.[54,55] This dibrominated complex provides aryl bromide handles that can be subjected to Sonogashira cross-coupling to extend conjugation of the system via addition of phenylacetylenes off the biladiene core that can be electron rich, deficient, or neutral. This synthetic strategy, which is illustrated in Figure 1b, generates a new family of **Pd[DMBil2–R]** compounds. Employing *para*-functionalized phenylacetylenes with electronically distinct functional groups,[66] provides a means to

further probe and tune the spectroscopic and $^1O_2$ sensitization properties of the **Pd[DMBil2–R]** complexes. These efforts provide a means to map how the electronics of the phenylacetylene appendages influence biladiene photophysics and support efforts directed toward eventual translation of biladiene photoagents for clinical use.

RESULTS AND DISCUSSION:

Pd[DMBilBr$_2$] was prepared according to previously reported methods.[28,33] New alkyne-appended **Pd[DMBil2–R]** derivatives were synthesized based on a modified published procedure that is summarized in Scheme 1. This procedure utilized tetrakis(triphenylphosphine)palladium(0), copper(I) iodide, the corresponding aryl-alkyne, and triethylamine in refluxing THF under inert atmosphere for 16 hours.[33,59,67,68] Phenylacetylenes that ranged from more electron-donating (R = NMe_2, OMe) to electron-withdrawing (CF_3, CN) were employed, and yields of synthesized compounds ranged from ~60–90% after chromatographic purifications. All **Pd[DMBil2–R]** products were characterized by ^{1}H, ^{13}C{^{1}H} , and ^{19}F NMR spectroscopy, as well as high-resolution mass spectrometry as detailed in the Supplementary Information (SI).

Scheme 1: Synthetic route employed to prepare **Pd[DMBil2–R]** derivatives.

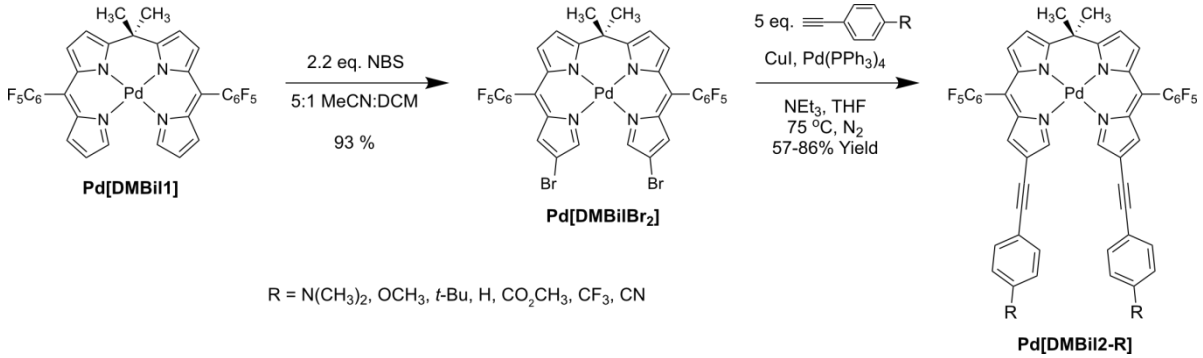

Single-crystal X-ray diffraction experiments enabled the full structural characterization of several of the **Pd[DMBil2–R]** derivatives (Figure 2). **Pd[DMBil2–H]** (Figure 2a), **Pd[DMBil2–OCH_3]** (Figure 2b), **Pd[DMBil2–CN]** (Figure 2c), and **Pd[DMBil2–CF_3]** (Figure 2d) were crystallized via slow evaporation from saturated methanol solutions (Figures S22–S25 in the SI include fully labelled structures). **Pd[DMBil2–H]** and **Pd[DMBil2–OCH_3]** showed a single asymmetric molecule within their respective unit cells, **Pd[DMBII2–CN]** is represented by three molecules with unique orientations and **Pd[DMBil2–CF_3]** is represented by two molecules with unique orientations. All solved structures show a clear axial and equatorial relationship of the sp^3 *meso*-carbons (C26 and C27) due to bowing of C10 outside of the pyrrole planes. Relevant crystallographic data are summarized in Table S1 of the SI.

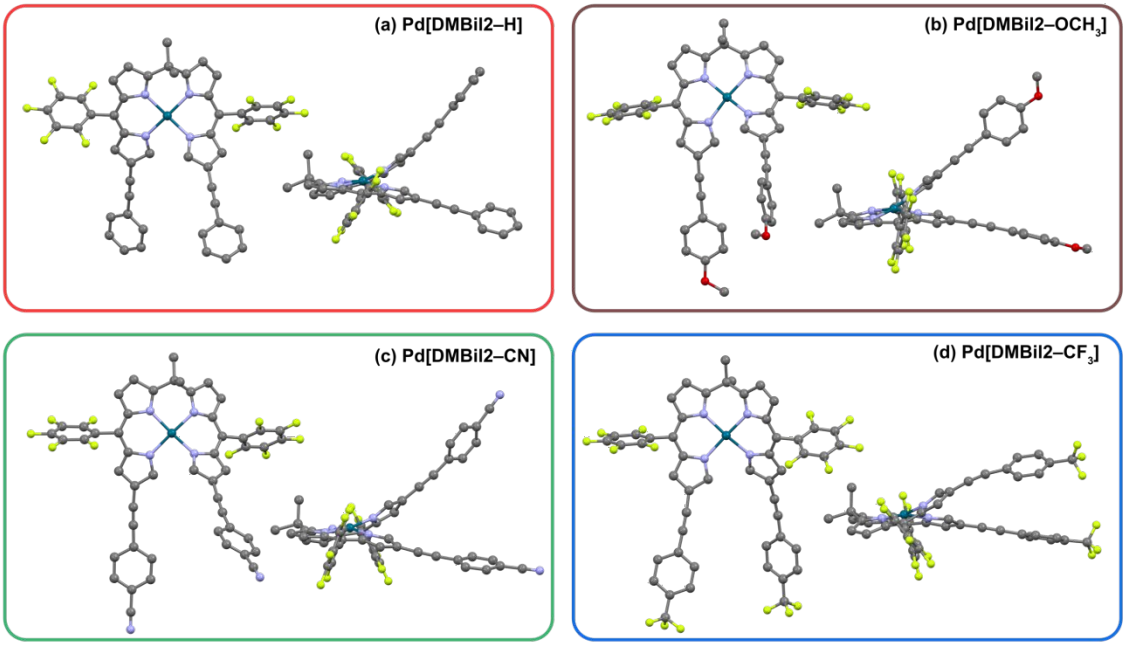

Figure 2: Ball and Stick representations of (a) **Pd[DMBil2–H]**, (b) **Pd[DMBil2–OCH_3]**, (c) **Pd[DMBil2–CN]**, and (d) **Pd[DMBil2–CF_3]** as viewed from top and in profile. Hydrogen atoms and disordered solvent molecules have been omitted for clarity.

For each of the X-ray structures, The Pd(II) metal centers coordinate to the four pyrrole units with slightly shorter Pd—N bond distances than observed for the parent **Pd[DMBil1]**. Values ranged from 1.982–2.046 Å for the **Pd[DMBil2–R]** derivatives versus the previously published 2.000–2.043 Å for **Pd[DMBil1]**.[22] The previous structures determined for **Pd[DMBil1]** derivatives revealed that the Pd(II) center did not conform to the expected square planar geometry common for four-coordinate d^8 metal complexes. This structural distortion is also observed for the new **Pd[DMBil2–R]** complexes, as demonstrated through calculation of their geometry indices (τ'_4). While the parent **Pd[DMBil1]** complex, showed $\tau'_4 = 0.109$, the geometry indices were determined as $\tau'_4 =$ 0.151, 0.140 and 0.153 for **Pd[DMBil2–H]**, **Pd[DMBil2–CF_3]**, and **Pd[DMBil2–OCH_3]**, respectively. Additionally, for the distinct **Pd[DMBil2–CN]** molecules in that crystal's unit cell, values of $\tau'_4 = 0.151$, 0.138, and 0.167 were found. All biladiene structures closely approach a square planar geometry, with a τ'_4 value near zero, however, the **Pd[DMBil2–H]** derivatives all showed larger τ'_4 values, indicating a slightly larger distortion toward seesaw coordination geometry ($\tau'_4 = 0.24$) as compared to the parent **Pd[DMBil1]**. The range of the geometry indices for **Pd[DMBil2–CN]** represent multiple stable structures and highlight the coordinative flexibility of the **Pd[DMBil2–R]** biladiene complexes.

The flexibility of **Pd[DMBil2–CN]** is evident from data presented in Table 1, which considers dihedral angles of the pyrrolic units, as well as the Ar–Pd–Ar angles between the Pd(II) center and the pendant arylalkynyl groups, which was determined from the profile views in Figure 2. The various planes of interest can be found in Figures S26–30 of the SI; the same atom numbering scheme was used for each biladiene derivative. The dihedral angle range of 17.65°–38.59° for the interior tetrapyrroles of **Pd[DMBil2–CN]**

highlights the flexibility of the sp^3-hybridized dipyrromethane backbone. The Ar–Pd–Ar angle also suggests a highly flexible ligand, as values ranged from 53.72° to 74.96° for the three different configurations. It is worth noting that the interior pyrrole dihedral angle for **Pd[DMBil2–H]** and **Pd[DMBil2–OCH_3]** are similar to each other (23.84° and 21.13°, respectively), while **Pd[DMBil2–CF_3]** shows greater flexibility, with angles of 31.19° and 36.44°. Overall, functionalizing the core **Pd[DMBil1]** scaffold with electronically distinct arylalkynes at the 2- and 18-positions does not drastically affect the geometric structures of the biladiene derivatives, though subtle deviations are apparent. As a whole, these results suggested to us that the new **Pd[DMBil2–R]** derivatives may show similar photochemical properties to the parent **Pd[DMBil1]** biladiene.

Table 1: Relevant dihedral angles for crystal structures of **Pd[DMBil2–CN]**, **Pd[DMBil2–CF_3]**, **Pd[DMBil2–H]**, and **Pd[DMBil2–OCH_3]**.

Dihedral Angles Between	Pd[DMBil2–CN]	Pd[DMBil2–CF_3]	Pd[DMBil2–H]	Pd[DMBil2–OCH_3]
interior pyrroles	25.50°, 38.59°, 17.65°	31.19°, 36.44°	23.84°	21.13°
terminal pyrroles	53.57°, 57.51°, 51.97°	50.07°, 49.48°	48.88°	48.62°
Dipyrromethene units and *meso* C_6F_5 groups	72.77°, 78.45°, 83.33°	86.19°, 81.56°	59.24°	70.68°
	78.41°, 80.76°, 62.25°	72.24°, 78.29°	66.95°	73.16°
Ar–Pd–Ar	74.96°, 71.08°, 51.62°	47.59°, 46.63°	50.36°	70.92°

UV-Visible absorption spectra of all **Pd[DMBil2–R]** derivatives were recorded in methanol and are shown in Figure 3 with λ_{max} listed in Table 2. Comparing the spectra recorded for **Pd[DMBil2–H]** and **Pd[DMBil1]** (Figure 3a), shows that both species have a similar absorption profile including a local λ_{max} near 405 nm. The two compounds differ in that **Pd[DMBil2–H]** shows a red-shift in λ_{max} by 35 nm and is extended into the

phototherapeutic window ~50 nm further than **Pd[DMBil1]**. The overall absorption for

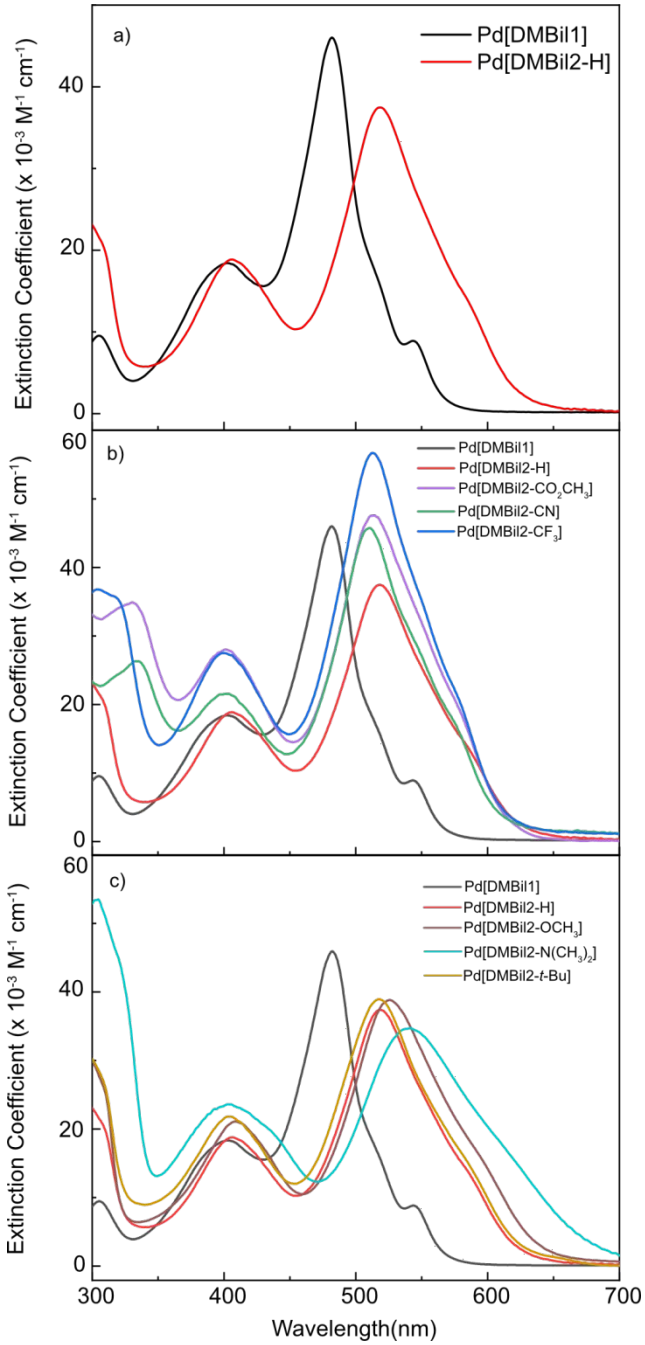

Figure 3: UV-Vis absorption spectra recorded in methanol of (a) **Pd[DMBil1]** versus **Pd[DMBil2–H]**, (b) electron-deficient **Pd[DMBil2–R]** derivatives (R = CN, CO_2Me, CF_3), and (c) electron-rich **Pd[DMBil2–R]** derivatives (OMe, NMe_2, *t*-Bu).

Pd[DMBil2–H] shows a slight increase in molar absorptivity at λ_{405} (ε_{405} = 18,900 $M^{-1}cm^{-1}$) compared to **Pd[DMBil1]** (ε_{405} = 17,400 $M^{-1}cm^{-1}$), but a decrease in molar absorptivity at λ_{max} (ε_{518} = 37,500 $M^{-1}cm^{-1}$) compared **Pd[DMBil1]** (ε_{483} = 45,300 $M^{-1}cm^{-1}$). Further, the low intensity peak that is observed at ~575 nm for **Pd[DMBil1]** exists as a slight shoulder on the low energy absorption band observed for **Pd[DMBil2–H]**. Extending the conjugation of the parent **Pd[DMBil1]** through coupling of phenyl acetylene red-shifted the biladiene's absorption profile and extended the low energy tail of the absorption spectrum from 600 nm (for **Pd[DMBil1]**) out to 650 nm for **Pd[DMBil2–H]**.

Table 2: Emission Data, including $^1O_2$ Quantum Yields recorded for **Pd[DMBil1]** and **Pd[DMBil2–R]** derivatives.

	σ_p	λ_{abs}/nm ($\varepsilon \times 10^3$ $M^{-1}cm^{-1}$)	λ_{fl}/nm (Φ_{fl})	λ_{ph}/nm (Φ_{ph})	Φ_Δ
[a]**Pd[DMBil1]**	------	483 (45.3)	557 (1.3×10^{-4})	753 (1.3×10^{-4})	57 %
Pd[DMBIl2–CN]	0.66	510 (45.8)	590 (7.5×10^{-4})	715 (5.8×10^{-5})	91 %
Pd[DMBil2–CF_3]	0.54	513 (56.7)	589 (8.2×10^{-4})	721 (1.6×10^{-4})	92 %
Pd[DMBil2–CO_2CH_3]	0.45	512 (47.6)	606 (7.8×10^{-4})	776 (1.8×10^{-4})	61 %
Pd[DMBil2–H]	0.00	518 (37.5)	601 (2.3×10^{-4})	801 (3.7×10^{-5})	58 %
Pd[DMBil2–^{t}Bu]	–0.20	518 (39.0)	571 (1.4×10^{-4})	789 (3.0×10^{-6})	30 %
Pd[DMBil2–OCH_3]	–0.27	525 (38.9)	623 (1.7×10^{-4})	------	21 %
Pd[DMBil2–$N(CH_3)_2$]	–0.83	541 (32.8)	583 (1.4×10^{-5})	------	7.2 %

All spectroscopic data were gathered in methanol solutions at 298K. [a]Data reproduced from reference 43.

Elaboration of the **Pd[DMBil2–H]** motif via incorporation of either electron-withdrawing or donating groups at the *para*-position of the aryl rings showed two trends in the absorption profiles of the **Pd[DMBil2–R]** derivatives. The absorption characteristics for each **Pd[DMBil2–R]** derivative is listed in Table 2 along with the corresponding *para*-Hammett value (σ_p) for each R-group. The most electron deficient variants (larger σ_p values) appear toward the top of Table 2 (yellow rows) and the most electron rich (more

negative σ_p values) are toward the bottom (blue rows). Several trends are evident from inspection of the spectroscopic properties across the collection of **Pd[DMBil2–R]** derivatives. The first trend is that the maximum extinction coefficient near 515 nm increases for the electron deficient aryl ring derivatives relative to **Pd[DMBil2–H]** (Figure 3b), with the most strongly absorbing variant being **Pd[DMBil2–CF_3]**, which presents ε_{513} = 56,700 $M^{-1}cm^{-1}$ (versus ε_{518} = 37,500 $M^{-1}cm^{-1}$ for **Pd[DMBil2–H]**). By contrast, installation of electron donating R-groups at the *para*-position does not have a substantial impact on the overall absorptivity at λ_{max}, however, a second trend is apparent from inspection of the UV-vis spectra compiled in Figure 3c. Upon functionalization with electron donating R-groups (*i.e.*, *t*-Bu, OMe, NMe_2), a distinct bathochromic shift of λ_{max} is plainly evident. The overall shift from electronically neutral (**Pd[DMBil2–H]**; λ_{max} = 518 nm) to the most electron rich (**Pd[DMBil2–$N(CH_3)_2$]**; λ_{max} = 541 nm) is greater than 20 nm (see Table 2 and Figure 3c). The manner in which these trends in λ_{max} and ε_{max} across all of the **Pd[DMBil2–R]** variants correlate with the σ_p values for the *para*- R-groups is discussed below (*vide infra*).

Photoluminescence studies were performed for each of the **Pd[DMBil2-R]** derivatives dissolved in MeOH at room temperature. Spectra were collected under N_2 following irradiation into the Soret-like absorption feature (λ_{exc} = 500 nm). Similar to the parent **Pd[DMBil1]** complex, each of the extended biladienes was weakly luminescent. Also similar to the parent **Pd[DMBil1]** complex, the **Pd[DMBil2-R]** complexes showed two pronounced emission features corresponding to fluorescence and phosphorescence, respectively.[69] Fluorescence bands ranged from λ_{fl} ~ 570 – 645 nm, while longer wavelength emission that was sensitive to the presence of O_2 (*i.e.*, phosphorescence)

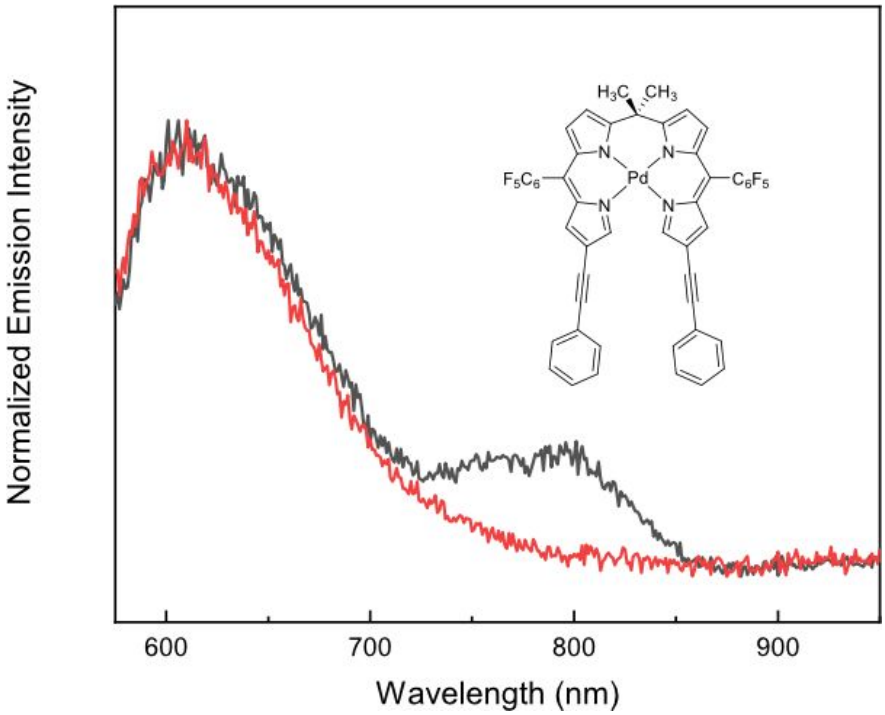

Figure 4: Emission spectra recorded in methanol for **Pd[DMBil2-H]** under inert atmosphere of N_2 (black) and after exposure to air (red).

was observed from λ_{ph} = 725 – 850 nm. The photoluminescence spectrum of **Pd[DMBil2–H]** is representative in this regard and is shown in Figure 4. Emission spectra for each of the **Pd[DMBil2–R]** derivatives are reproduced in Figure S32.

The intensity of photoluminescence varied for each of the **Pd[DMBil2–R]** complexes. With respect to fluorescence, the electronically neutral **Pd[DMBil2–H]** complex was determined to have a fluorescence quantum yield of $\Phi_{fl} = 2.3 \times 10^{-4}$, which is very similar to that of **Pd[DMBil1]** ($\Phi_{fl} = 1.3 \times 10^{-4}$). For the rest of the **Pd[DMBil2–R]** derivatives, the fluorescence quantum yields ranged from $\Phi_{fl} = 1.4 \times 10^{-5}$ for **Pd[DMBil2–N(CH$_3$)$_2$]** to 8.2×10^{-4} for **Pd[DMBil2–CF$_3$]** (Table 2). As described in greater detail below (*vide infra*) extended biladienes bearing electron-withdrawing R-groups displayed a slight increase in fluorescence quantum yield versus the parent **Pd[DMBil1]**, while the more electron rich variants were less strongly emitting.

The identity of the biladiene R-group more strongly influences the intensity of phosphorescence. Triplet emission could only be clearly detected for electron-deficient (R = CN, CF_3, CO_2Me), electronically-neutral (R = H) or slightly electron-rich (R = ^{t}Bu) **Pd[DMBil2–R]** species. These compounds for which the corresponding σ_p values are at least –0.20 (Table 2) showed a clear broad phosphorescent feature at λ_{ph} ~ 725–850 nm under inert atmosphere. Quantum yields for phosphorescence for these compounds ranged from Φ_{ph} ~ 3×10^{-6} to 2×10^{-4} (See Table 2). All the electron-deficient species displayed similar Φ_{ph} values and the two most electron rich variants (R = OMe and NMe_2) did not phosphoresce at room temperature (Figure S32, Table 2). While σ_p and Φ_{ph} values are not strongly correlated in a linear sense, it is clear that installation of the most electron-rich aryl alkynes on the biladiene backbones perturbs the tetrapyrrole photophysics such that triplet emission is not observed.

To fully capture the overall electronic effects of alkynyl-arene substitution on the spectroscopic properties of the **Pd[DMBil2–R]** complexes, the UV-Vis absorption and fluorescence characteristics for each biladiene were analyzed as a function of the *para*-Hammett parameter value (σ_p) for the R-group on the arylalkyne appendage. Correlations with respect to UV-vis absorption (λ_{max}, ε_{max}) and Φ_{fl} versus σ_p are provided in Figure 5a-c. A clear inverse relationship is observed for values of λ_{max} (Figure 5a) upon moving from electron-rich to electron-deficient R-groups, as absorption spectra are most strongly red-shifted upon installation of electron-donating R-groups at the expense of ε_{max}. Conversely, a positive correlation is observed for ε_{max} values relative to σ_p. Although the biladiene absorption spectra are slightly blue-shifted upon introduction of electron-deficient R-groups, these compounds absorb much more strongly at their λ_{max} near 525 nm. For the

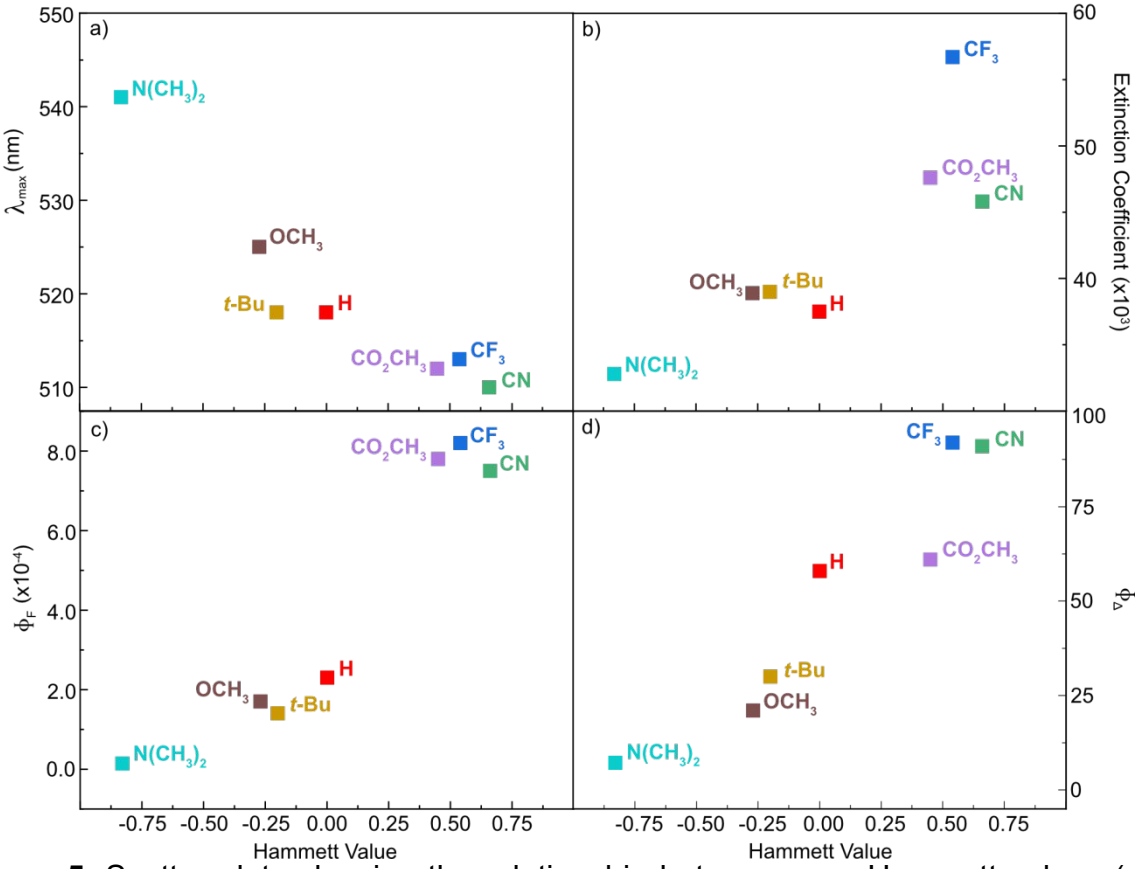

Figure 5: Scatter plots showing the relationship between *para*-Hammett values (σ_p) and (a) absorption maximum (λ_{max}), (b) molar absorptivity (ε_{max}), (c) fluorescence quantum yield (Φ_{fl}), and (d) $^1O_2$ quantum yield (Φ_Δ).

case of the fluorescence quantum yields, there is a positive correlation with the σ_p values (Figure 5c); Φ_{fl} increases as the arylalkyne R-group is varied from electron-donating to electron-neutral to electron-withdrawing. In sum, as arylalkyne groups become more electron rich, biladiene emission becomes less efficient.

For the each of the phosphorescent **Pd[DMBil2–R]** derivatives, long-wavelength emission was diminished upon exposure to air (see Figure 4), suggesting that the **Pd[DMBil2–R]** complexes can sensitize the formation of $^1O_2$ with appreciable quantum yields. Methylene blue was used as an actinometer (Φ_Δ = 51% in methanol) to determine the quantum yields of $^1O_2$ formation (Φ_Δ) upon irradiation with λ_{exc} = 600 nm. Singlet

oxygen sensitization experiments utilized 1,3-diphenylisobenzofuran (DPBF) as a $^1O_2$ probe. **Pd[DMBil2–H]** displayed an appreciable quantum yield of Φ_Δ = 58%, which is nearly identical to that for the parent **Pd[DMBil1]** when excited at 500 nm (Φ_Δ = 57%). This result demonstrates that addition of arylalkyne functionalities on the biladiene periphery does not inherently diminish the ability of palladium biladiene frameworks to sensitize triplet chemistry. Moreover, **Pd[DMBil2–H]** offers advantages over the parent **Pd[DMBil1]** complex for photomedicine applications because it can be excited using tissue penetrating red-light from the phototherapeutic window.

Each of the other **Pd[DMBil2–R]** derivatives also showed ability to sensitize formation of $^1O_2$, as summarized in Table 2. Notably, as electron deficient R-groups are installed on the biladiene arylalkyne appendages, the efficiency of singlet oxygen sensitization increases dramatically. **Pd[DMBil2–CO_2Me]** featured a slight increase in Φ_Δ to above 60%, but the most electron-deficient variants (**Pd[DMBil2–CN]** and **Pd[DMBil2–CF_3]**) display Φ_Δ efficiencies above 90%, which are the highest recorded to date for biladiene complexes. By contrast, the extended biladiene derivatives bearing the most electron-rich R-groups (OMe and NMe_2) (*i.e.*, those that did not phosphoresce), were poor sensitizers of $^1O_2$, despite featuring the most red-shifted UV-vis absorption spectra (Table 2). These observations suggest that **Pd[DMBil2–OCH_3]** and **Pd[DMBil2–$N(CH_3)_2$]**, either do not efficiently cross over to the triplet excited state due to enhanced non-radiative deactivation from the S_1 state, or have much shorter-lived triplet excited states, which circumvents the energy transfer process needed to generate $^1O_2$.

On the whole, there is a clear positive Hammett correlation for values of Φ_Δ (Figure 5d) upon moving from electron-donating to electron-withdrawing R-groups. As the

alkynyl-arene substitution is varied, an increase in $^1O_2$ quantum yield, from ~7 % (for **Pd[DMBil2–N(CH$_3$)$_2$]**) to >90 % (for **Pd[DMBil2–CF$_3$]**) is observed (Figure 5d). This trend is reminiscent of that detailed for Φ_{fl}, in which more electron-rich biladienes were less emissive, presumably due to improved non-radiative decay being operative for the biladienes featuring electron-rich aryl moieties.

One potential non-radiative pathway that could serve to deactivate **Pd[DMBil2–R]** derivatives from either singlet or triplet excited states involves intramolecular charge transfer from the arylalkyne units to the biladiene core. To better assess whether such deactivation pathways are feasible, we determined how the redox behavior of the **Pd[DMBil2–R]** derivatives is influenced by variation in the R-groups. Cyclic voltammetry (CV) and differential pulsed voltammetry (DPV) experiments were carried out in acetonitrile solutions containing each **Pd[DMBil2–R]** derivative (1 mM) and 100 mM $TBAPF_6$ as supporting electrolyte. Measured redox potentials are compiled in Table 3 (redox values are based on DPVs shown in Figure S39). Figure 6 also reproduces CV traces for **Pd[DMBil1]** and each of the **Pd[DMBil2–R]** derivatives.

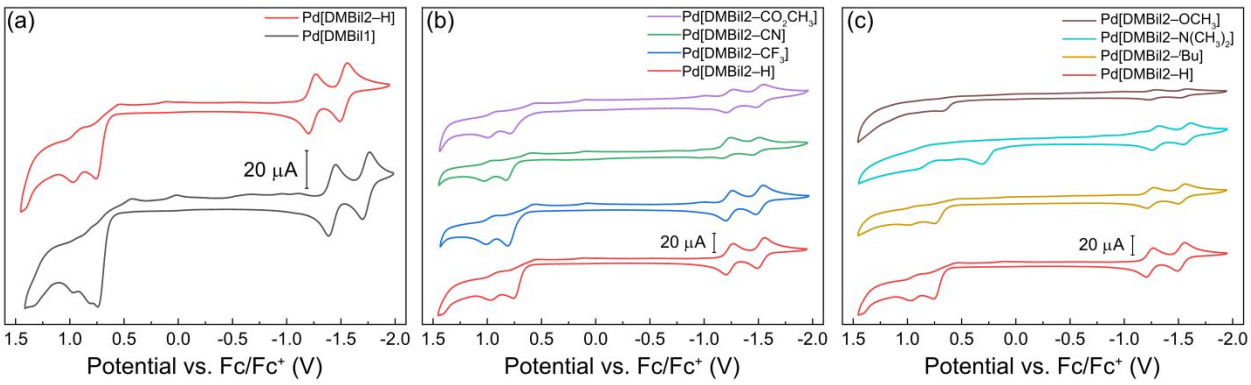

Figure 6: Cyclic voltammograms recorded for (a) **Pd[DMBil1]** and **Pd[DMBil2–H]**, (b) **Pd[DMBil2–H]** and **Pd[DMBil2–R]** derivatives bearing electron-withdrawing R-groups, (c) **Pd[DMBil2–H]** and **Pd[DMBil2–R]** derivatives bearing electron-donating R-groups, in anhydrous acetonitrile containing 0.1 M $TBAPF_6$ under Ar. Data were collected using a glassy carbon disk working electrode, platinum mesh counter electrode and Ag/AgCl reference electrode, at a scan rate of 100 mV s^{-1}. All data are referenced to Fc/Fc^+.

The parent **Pd[DMBil1]** complex exhibited two quasi-reversible reduction waves (–1.39, –1.71 V) and two irreversible oxidation waves (+0.84, +0.51 V). All potentials herein are reported versus Fc/Fc^+. The voltammograms for **Pd[DMBil2–H]** (Figures 6a and S33) are similar to that for **Pd[DMBil1]**, displaying multiple irreversible oxidation waves (+0.99 and +0.59 V) and two quasi-reversible reduction waves (–1.23 and –1.52 V). Notably, based on these potentials, the electron-neutral extended biladiene (**Pd[DMBil2–H]**) is slightly more difficult to oxidize (by ~ 150 mV) and easier to reduce (by ~ 200 mV) relative to **Pd[DMBil1]**. These results demonstrate that extending the π–conjugation of the biladiene ligand scaffold perturbs the tetrapyrrole's redox properties. The delocalization of electrons and inductive electron-withdrawing effect of the aryl alkynyl moiety facilitates biladiene reduction but makes oxidation of the tetrapyrrole core more difficult.

Table 3: Electrochemical data and $^1O_2$ sensitization efficiencies recorded for **Pd[DMBil1]** and **Pd[DMBil2–R]** derivatives.

	σ_p	E_{ox} (vs. Fc/Fc^+) (V)	E_{red} (vs. Fc/Fc^+) (V)	Φ_Δ
Pd[DMBil1]	------	0.84, 0.51	–1.39, –1.71	57%
Pd[DMBIl2–CN]	0.66	1.00, 0.66	–1.18, –1.46	91%
Pd[DMBil2–CF_3]	0.54	1.03, 0.65	–1.22, –1.50	92%
Pd[DMBil2–CO_2CH_3]	0.45	0.98, 0.63	–1.21, –1.49	61%
Pd[DMBil2_H]	0.00	0.99, 0.59	–1.23, –1.52	58%
Pd[DMBil2–^{t}Bu]	–0.20	0.99, 0.60	–1.22, –1.51	30%
Pd[DMBil2–OCH_3]	–0.27	0.93, 0.55	–1.24, –1.53	21%
Pd[DMBil2–$N(CH_3)_2$]	–0.83	0.70, 0.33	–1.27, –1.57	7.2%

The redox behavior for the substituted **Pd[DMBil2–R]** derivatives revealed similar single-electron redox behavior as compared to unsubstituted **Pd[DMBil2–H]** (Figure 6b). As might be expected, the nature of the biladiene R-group impacts the oxidation and reduction potentials of the extended biladiene. As shown by the data in Table 3, a positive

shift in reduction potential by ~10–50 mV is observed when electron withdrawing groups (*i.e.,* CN, CF_3, CO_2CH_3) are installed on the extended biladiene. The potential differences, though small, indicate that the presence of electron-withdrawing *para*-substituents facilitate reduction. The presence of electron-withdrawing groups also results in an increase of oxidation potential in all cases by ~30 mV (see Table 3 and Figure 6b). Generally speaking, the stronger the electron-withdrawing capabilities of the substituent, the greater the shift in both oxidation and reduction potentials relative to **Pd[DMBil2–H]**.

While there are virtually no differences between **Pd[DMBil2–H]** and **Pd[DMBil2–^{t}Bu]** in terms of redox behavior, the extended biladienes bearing strongly donating groups (*i.e.*, OMe and NMe_2) are characterized by considerably different cyclic voltammograms (Figure 6c). While both derivatives retain two quasi-reversible single-electron reduction waves, only a single oxidation event (0.33 V) (along with a less distinct feature at 0.70 V) was observed for **Pd[DMBil2–NMe_2]**. Along similar lines a small oxidation wave was observed for **Pd[DMBil2–OCH_3]** at 0.55 V. For these complexes bearing strongly electron-releasing R-groups, it is possible that oxidation of the *para*-substituent is

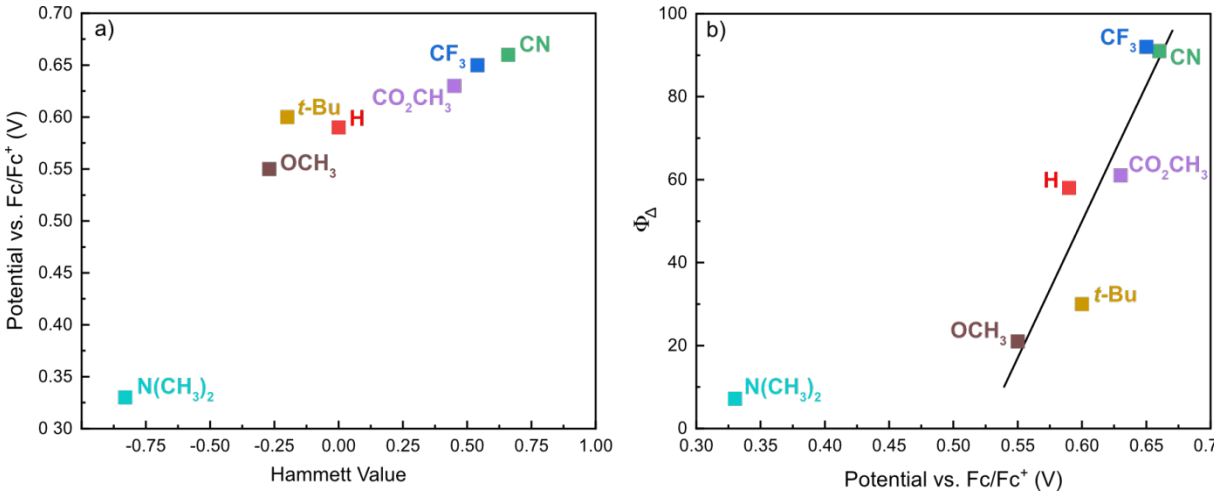

Figure 7: Scatter plots showing the relationship between the first oxidation potential of each **Pd[DMBil2–R]** derivative and (a) the corresponding *para*-Hammett values (σ_p), and (b) the corresponding $^1O_2$ quantum yields (Φ_Δ).

occurring before ligand oxidation. As compared to **Pd[DMBil2–H]**, **Pd[DMBil2–NMe$_2$]** is more difficult to reduce by ~30–40 mV (–1.27, –1.57 V) and is much easier to oxidize, as would be expected upon introduction of very strong electron-donating substituents.

While the most prominent differences in redox behavior are observed between **Pd[DMBil1]** and the suite of **Pd[DMBil2–R]** derivatives, the ease of oxidation/reduction for the family of extended biladiene derivatives is influenced by the R-group on the aryl-alkyne units. As shown in Figure S34, both of the oxidation and reduction events for each **Pd[DMBil2–R]** derivative corelates with the σ_p values for the R-group on the aryl groups of the extended biladienes. The relation of the first oxidation potential for each **Pd[DMBil2–R]** derivative to the corresponding R-group σ_p values is also shown in Figure 7a.

One potential non-radiative pathway that could serve to deactivate **Pd[DMBil2–R]** derivatives from either the singlet or triplet excited state involves intramolecular charge transfer from the arylalkyne units to the biladiene core. This inference is bolstered by noting that for the electron–rich **Pd[DMBil2–OCH$_3$]** and **Pd[DMBil2–NMe$_2$]** derivatives, a sharp decline in singlet O_2 sensitization efficiency is observed (Table 2). Notably, these are the two extended biladienes that show the lowest oxidation potentials (Table 3). By contrast, the most electron deficient **Pd[DMBil2–CN]** and **Pd[DMBil2–CF$_3$]** derivatives, which are the most thermodynamically challenging to oxidize, support $^1O_2$ quantum yields that are above 90%.

To qualitatively test the above supposition, we considered what effect protonation of the dimethylamine groups of **Pd[DMBil2–NMe$_2$]** would have on the compound's photochemical properties. While –NMe$_2$ functionalities are strongly electron-donating (σ_p

= –0.83), protonation to generate $–NHMe_2^+$ results in an aryl substituent that is strongly electron-withdrawing ($\sigma_p \sim 0.7$),[66] suggesting **Pd[DMBil2–NMe$_2$]** should support a less red-shifted absorption spectrum and higher $^1O_2$ sensitization efficiency in the presence of acid. Titration of a 20 μM solution of **Pd[DMBil2–NMe$_2$]** in MeOH with upto 500 equivalents of trifluoroacetic acid drives the full protonation of both $–NMe_2$ groups as evidenced by stacked absorption spectra shown in Figure S35. Protonation of the dimethylamine groups drives a shift in the biladiene's absorption spectra to the blue from λ_{max} = 541 nm for the parent **Pd[DMBil2–NMe$_2$]** to λ_{max} = 520 nm. Similarly, while **Pd[DMBil2–NMe$_2$]** is a poor sensitizer of $^1O_2$ (Φ_Δ = 7.2%) upon full protonation, we observe an increase of $^1O_2$ sensitation efficienty to Φ_Δ = 85.3%. These results reinforce the observed trend that extended biladienes bearing electron-withdrawing substituents (*i.e.*, $–NHMe_2^+$) will support less redshifted absorbance profiles and higher singlet oxygen quantum yields as compared to biladienes bearing electron-donating groups (*i.e.*, $–NMe_2$).

The extent to which the Φ_Δ values and oxidation potentials are connected for the most electron-rich and deficient extended biladienes suggests that the quantum efficiency of $^1O_2$ sensitization observed for each **Pd[DMBil2–R]** derivative may reflect the ease with which the extended biladienes can be oxidized. Figure 7b demonstrates that a good linear correlation exists between the first oxidation potential and the σ_p values for all but one of the **Pd[DMBil2–R]** derivatives (i.e., **Pd[DMBil2–NMe$_2$]**). This overall trend is not entirely suprising since both the first oxidation potentials and Φ_Δ values for each extended biladiene correlate with the σ_p values for the arylalkyne R-groups (vide supra). The linear regression shown in Figure 7b projects a Φ_Δ value of ~10% for a **Pd[DMBil2–R]** derivative

that can be oxidized at E ~ 0.53 V versus Fc/Fc+. Based on this regression, we would expect that any biladiene derivative that is oxidized at potentials below 0.53 V would demonstrate a Φ_Δ value below 10%. Based on this analysis, the low effiency with which **Pd[DMBil2–NMe$_2$]** sensitizes the formation of $^1O_2$ and the placement of the data point corresponding to this derivative in Figure 7b are readily rationalized.

CONCLUSIONS AND FUTURE DIRECTIONS:

The continued interest in developing efficacious and synthetically accessible photosensitizers for PDT inspires efforts to prepare and characterize new tetrapyrrole complexes. Although prior work in our group has establshed **Pd[DMBil1]** as an efficient photosensitizer of $^1O_2$ and **Pd[DMBil1]–PEG$_{750}$**, as a capable photoagent for PDT in cell culture, these first generation biladienes do not absorb within the phototherapeutic window of 600 to 900 nm, which limits translational efforts. In addressing this limitation, we have developed an efficient route to extended biladiene derivatives that bear alkynylaryl groups at the 2- and 18-positions. These extended tetrapyrroles are prepared in modular fashion through Sonogashira coupling of appropriate alkynes with **Pd[DMBilBr$_2$]** to deliver a suite of **Pd[DMBil2–R]** derivatives in which electron-donating, electronically neutral, or electron-withdrawing R-groups are appended on to the arylalkyne moieties. The electronic nature of the R-groups provides a means to tune spectroscopic, photophysical, and redox properties of the extended biladiene architectures.

All newly-synthesized **Pd[DMBil2–R]** derivatives showed at least slight absorption enhancement past 600 nm. **Pd[DMBil2–R]** derivatives bearing a more electron-rich

arylalkynes display absorption spectra that are shifted to longer wavelengths well past 600 nm. The largest shift was observed for the extended biladiene bearing dimethylamine groups (**Pd[DMBil2–N(CH_3)$_2$]**), which absorb light out to ~700 nm. The steady-state spectroscopic properties of the biladienes correlate with the Hammet parameter (σ_p) for the R-group installed on the arylalkyne moiety; **Pd[DMBil2–R]** molar absorptivity and fluorescence quantum yield are positively correlated while the absorption maxima are negatively correlated (see Figure 5). The redox behavior for the extended biladienes is also sensitive to the electronic nature of the arylalkyne R-group. In particular, the first oxidation potentials recorded for the suite of **Pd[DMBil2–R]** complexes also shows some correlation with R-group Hammet parameter and range from E_{ox} ~ 0.70 V for the most electron rich biladiene (**Pd[DMBil2–N(CH_3)$_2$]**) to E_{ox} ~ 1.03 V for the most electron deficient (**Pd[DMBil2–CF_3]**).

Since each **Pd[DMBil2–R]** derivative absorbed light in the phototherapeutic window, $^1O_2$ quantum yields (Φ_Δ) were measured for each compound. Extended biladienes containing electron withdrawing R-groups (*i.e.,* R= CN, CF_3) supported higher Φ_Δ values, with the most electron deficient variants (**Pd[DMBil2–CN]** and **Pd[DMBil2–CF_3]**) surpassing 90%. These two complexes represent the most efficient biladiene based $^1O_2$ sensitizers prepared to date. The most electron-rich extended biladiene (**Pd[DMBil2–N(CH_3)$_2$]**) is a relatively poor sensitizer of $^1O_2$ (Φ_Δ < 10%). Like the other steady-state spectroscopic properties, extended biladiene $^1O_2$ sensitization efficiency is also correlated with the electronic nature of the arylalkyne R-group. A general positive correlation is observed between the recorded Φ_Δ values and the R-group σ_p values (Figure 5). In general, **Pd[DMBil2–R]** derivatives with arylalkyne groups corresponding to

σ_p > 0.0 (i.e., R= H) offer improved $^1O_2$ quantumn yields relative to the first generation **Pd[DMBil1].**

Considering the opposing trends in **Pd[DMBil2–R]** absorption and $^1O_2$ sensitization efficiency demonstrates that a delicate interplay exists between achieving red-shifted biladiene-based phototherapeutic agents that are capable of generating singlet oxygen with good efficiency. In sum, extending the π-conjugation by adding unsaturated moieties is a productive strategy to establish biladienes that can more strongly absorb tissue penetrating light and maintaining an electron-deficient oligotetrapyrrole core appears neccessary for biladienes to be highly efficient $^1O_2$ sensitizers. Based on the above findings, future work from our laboratory will establish whether similar trends hold upon extension of the biladiene core with π-conjugated moieties other than arylalkynes and assess how **Pd[DMBil2–R]** complexes and future generations of extended biladienes perform as phototherapeutic agents in cell culture and animal models.

Corresponding Author

* E-mail: joelr@udel.edu

Conflicts of interest

There are no conflicts to declare.

Associated content

Supporting Information. Synthetic procedures as well as additional spectral and characterization data are found in the Supporting Information.

Acknowledgements

Portions of the tetrapyrrole synthetic work were supported through the U.S. Department of Energy, Office of Science, Office of Basic Energy Sciences EPSCoR and Catalysis programs under Award Number DESC-0001234 (J.R.). Research reported in this publication was also supported by the National Institute Of General Medical Sciences of the National Institutes of Health under Award Number T32GM133395. The content is solely the responsibility of the authors and does not necessarily represent the official views of the National Institutes of Health.

REFERENCES

1 P. Agostinis, K. Berg, K. A. Cengel, T. H. Foster, A. W. Girotti, S. O. Gollnick, S. M. Hahn, M. R. Hamblin, A. Juzeniene, D. Kessel, M. Korbelik, J. Moan, P. Mroz, D. Nowis, J. Piette, B. C. Wilson and J. Golab, *CA. Cancer J. Clin.*, 2011, **61**, 250–281.

2 A. F. dos Santos, D. R. Q. de Almeida, L. F. Terra, M. S. Baptista and L. Labriola, *J. Cancer Metastasis Treat.*, 2019, **5**, 25.

3 D. E. J. G. J. Dolmans, D. Fukumura and R. K. Jain, *Nat. Rev. Cancer*, 2003, **3**, 380–387.

4 E. Sorbellini, M. Rucco and F. Rinaldi, *Lasers Med. Sci.*, 2018, **33**, 1431–1439.

5 M. J. Davies, *Biochem. Biophys. Res. Commun.*, 2003, **305**, 761–770.

6 D. I. Pattison, A. Suryo Rahmanto and M. J. Davies, *Photochem. Photobiol. Sci.*, 2012, **11**, 38–53.

7 A. P. Castano, T. N. Demidova and M. R. Hamblin, *Photodiagnosis Photodyn. Ther.*, 2004, **1**, 279–293.

8 J. P. Celli, B. Q. Spring, I. Rizvi, C. L. Evans, K. S. Samkoe, S. Verma, B. W. Pogue and T. Hasan, *Chem. Rev.*, 2010, **110**, 2795–2838.

9 T. D. Mody and J. L. Sessler, *J. Porphyr. Phthalocyanines*, 2001, **05**, 134–142.

10 A. Kamkaew, S. H. Lim, H. B. Lee, L. V. Kiew, L. Y. Chung and K. Burgess, *Chem. Soc. Rev.*, 2012, **42**, 77–88.

11 T. Yogo, Y. Urano, Y. Ishitsuka, F. Maniwa and T. Nagano, *J. Am. Chem. Soc.*, 2005, **127**, 12162–12163.

12 S. Monro, K. L. Colón, H. Yin, J. I. Roque, P. Konda, S. Gujar, R. P. Thummel, L. Lilge, C. G. Cameron and S. A. McFarland, *Chem. Rev.*, 2019, **119**, 797–828.

13 F. Heinemann, J. Karges and G. Gasser, *Acc. Chem. Res.*, 2017, **50**, 2727–2736.

14 J. K. White, R. H. Schmehl and C. Turro, *Inorganica Chim. Acta*, 2017, **454**, 7–20.

15 M. C. DeRosa and R. J. Crutchley, *Coord. Chem. Rev.*, 2002, **233–234**, 351–371.

16 H. Abrahamse and M. R. Hamblin, *Biochem. J.*, 2016, **473**, 347–364.

17 A. B. Ormond and H. S. Freeman, *Materials*, 2013, **6**, 817–840.

18 D. Kessel, *J. Clin. Med.*, 2019, **8**, 1581.

19 A. E. O'Connor, W. M. Gallagher and A. T. Byrne, *Photochem. Photobiol.*, 2009, **85**, 1053–1074.

20 M. Ballico, V. Rapozzi, L. E. Xodo and C. Comuzzi, *Eur. J. Med. Chem.*, 2011, **46**, 712–720.

21 F. Giuntini, V. M. Chauhan, J. W. Aylott, G. A. Rosser, A. Athanasiadis, A. Beeby, A. J. MacRobert, R. A. Brown and R. W. Boyle, *Photochem. Photobiol. Sci.*, 2014, **13**, 1039–1051.

22 A. M. Potocny, A. J. Pistner, G. P. A. Yap and J. Rosenthal, *Inorg. Chem.*, 2017, **56**, 12703–12711.

23 N. V. Koudinova, J. H. Pinthus, A. Brandis, O. Brenner, P. Bendel, J. Ramon, Z. Eshhar, A. Scherz and Y. Salomon, *Int. J. Cancer*, 2003, **104**, 782–789.

24 A.-R. Azzouzi, E. Barret, C. M. Moore, A. Villers, C. Allen, A. Scherz, G. Muir, M. de Wildt, N. J. Barber, S. Lebdai and M. Emberton, *BJU Int.*, 2013, **112**, 766–774.

25 R. Baskaran, J. Lee and S.-G. Yang, *Biomater. Res.*, 2018, **22**, 25.

26 A. J. Pistner, G. P. A. Yap and J. Rosenthal, *J. Phys. Chem. C*, 2012, **116**, 16918–16924.

27 A. J. Pistner, D. A. Lutterman, M. J. Ghidiu, Y.-Z. Ma and J. Rosenthal, *J. Am. Chem. Soc.*, 2013, **135**, 6601–6607.

28 A. J. Pistner, D. A. Lutterman, M. J. Ghidiu, E. Walker, G. P. A. Yap and J. Rosenthal, *J. Phys. Chem. C*, 2014, **118**, 14124–14132.

29 A. M. Bruce, E. S. Weyburne, J. T. Engle, C. J. Ziegler and G. R. I. Geier, *J. Org. Chem.*, 2014, **79**, 5664–5672.

30 D. Kim, H.-J. Chun, C. C. Donnelly and G. R. I. Geier, *J. Org. Chem.*, 2016, **81**, 5021–5031.

31 R. Costa, G. R. Geier and C. J. Ziegler, *Dalton Trans.*, 2011, **40**, 4384–4386.

32 G. Pomarico, X. Xiao, S. Nardis, R. Paolesse, F. R. Fronczek, K. M. Smith, Y. Fang, Z. Ou and K. M. Kadish, *Inorg. Chem.*, 2010, **49**, 5766–5774.

33 M. Hoffmann, B. Cordes, C. Kleeberg, P. Schweyen, B. Wolfram and M. Bröring, *Eur. J. Inorg. Chem.*, 2016, **2016**, 3076–3085.

34 M. I. Martin, Q. Cai, G. P. A. Yap and J. Rosenthal, *Inorg. Chem.*, 2020, **59**, 18241–18252.

35 M. R. J. Marek, T.-N. Pham, J. Wang, Q. Cai, G. P. A. Yap, E. S. Day and J. Rosenthal, *ACS Omega*, 2022, **7**, 36653–36662.

36 J.-M. Benech, L. Bonomo, E. Solari, R. Scopelliti and C. Floriani, *Angew. Chem. Int. Ed.*, 1999, **38**, 1957–1959.

37 B. Dolenský, J. Kroulík, V. Král, J. L. Sessler, H. Dvořáková, P. Bouř, M. Bernátková, C. Bucher and V. Lynch, *J. Am. Chem. Soc.*, 2004, **126**, 13714–13722.

38 P. Pushpanandan, Y. K. Maurya, T. Omagari, R. Hirosawa, M. Ishida, S. Mori, Y. Yasutake, S. Fukatsu, J. Mack, T. Nyokong and H. Furuta, *Inorg. Chem.*, 2017, **56**, 12572–12580.

39 J. L. Sessler, R. S. Zimmerman, C. Bucher, V. Král and B. Andrioletti, *Pure Appl. Chem.*, 2001, **73**, 1041–1057.

40 A. J. Pistner, R. C. Pupillo, G. P. A. Yap, D. A. Lutterman, Y.-Z. Ma and J. Rosenthal, *J. Phys. Chem. A*, 2014, **118**, 10639–10648.

41 S. P. Zakharova, E. V. Rumyantsev and E. V. Antina, *Russ. J. Coord. Chem.*, 2005, **31**, 849–855.

42 A. Savoldelli, R. Paolesse, F. R. Fronczek, K. M. Smith and M. G. H. Vicente, *Org. Biomol. Chem.*, 2017, **15**, 7255–7257.

43 S. M. Martin, G. M. Repa, R. C. Hamburger, C. A. Pointer, K. Ward, T.-N. Pham, M. I. Martin, J. Rosenthal, L. A. Fredin and E. R. Young, *Phys. Chem. Chem. Phys.*, 2023, **25**, 2179–2189.

44 Q. Cai, A. T. Rice, C. A. Pointer, M. I. Martin, B. Davies, A. Yu, K. Ward, P. R. Hertler, M. C. Warndorf, G. P. A. Yap, E. R. Young and J. Rosenthal, *Inorg. Chem.*, 2021, **60**, 15797–15807.

45 A. M. Potocny, R. S. Riley, R. K. O'Sullivan, E. S. Day and J. Rosenthal, *Inorg. Chem.*, 2018, **57**, 10608–10615.

46 R. S. Riley, R. K. O'Sullivan, A. M. Potocny, J. Rosenthal and E. S. Day, *Nanomaterials*, 2018, **8**, 658.

47 J. Wang, A. M. Potocny, J. Rosenthal and E. S. Day, *ACS Omega*, 2020, **5**, 926–940.

48 K. Hanson, L. Roskop, P. I. Djurovich, F. Zahariev, M. S. Gordon and M. E. Thompson, *J. Am. Chem. Soc.*, 2010, **132**, 16247–16255.

49 H. Imahori, T. Umeyama and S. Ito, *Acc. Chem. Res.*, 2009, **42**, 1809–1818.

50 K. Hara, T. Sato, R. Katoh, A. Furube, Y. Ohga, A. Shinpo, S. Suga, K. Sayama, H. Sugihara and H. Arakawa, *J. Phys. Chem. B*, 2003, **107**, 597–606.

51 N. Kobayashi, H. Ogata, N. Nonaka and E. A. Luk'yanets, *Chem. – Eur. J.*, 2003, **9**, 5123–5134.

52 D. Qi, L. Zhang, Y. Zhang, Y. Bian and J. Jiang, *J. Phys. Chem. A*, 2010, **114**, 13411–13417.

53 J. E. Rogers, K. A. Nguyen, D. C. Hufnagle, D. G. McLean, W. Su, K. M. Gossett, A. R. Burke, S. A. Vinogradov, R. Pachter and P. A. Fleitz, *J. Phys. Chem. A*, 2003, **107**, 11331–11339.

54 A. T. Rice, M. I. Martin, M. C. Warndorf, G. P. A. Yap and J. Rosenthal, *Inorg. Chem.*, 2021, **60**, 11154–11163.

55 A. T. Rice, G. P. A. Yap and J. Rosenthal, *Photochem*, 2022, **2**, 58–68.

56 P. Yadav, M. Sankar, X. Ke, L. Cong and K. M. Kadish, *Dalton Trans.*, 2017, **46**, 10014–10022.

57 R. Kumar and M. Sankar, *Inorg. Chem.*, 2014, **53**, 12706–12719.

58 M. Taniguchi, D. L. Cramer, A. D. Bhise, H. L. Kee, D. F. Bocian, D. Holten and J. S. Lindsey, *New J. Chem.*, 2008, **32**, 947–958.

59 J. Rosenthal, E. R. Young and D. G. Nocera, *Inorg. Chem.*, 2007, **46**, 8668–8675.

60 H. Langhals, *Angew. Chem. Int. Ed.*, 2004, **43**, 5291–5292.

61 T. Chandra, B. J. Kraft, J. C. Huffman and J. M. Zaleski, *Inorg. Chem.*, 2003, **42**, 5158–5172.

62 F. Ponsot, N. Desbois, L. Bucher, M. Berthelot, P. Mondal, C. P. Gros and A. Romieu, *Dyes Pigments*, 2019, **160**, 747–756.

63 J. T. Fletcher and M. J. Therien, *J. Am. Chem. Soc.*, 2002, **124**, 4298–4311.

64 T. Tanaka and A. Osuka, *Chem. Soc. Rev.*, 2015, **44**, 943–969.

65 D. P. Arnold and D. A. James, *J. Org. Chem.*, 1997, **62**, 3460–3469.

66 Corwin. Hansch, A. Leo and R. W. Taft, *Chem. Rev.*, 1991, **91**, 165–195.

67 A. A. S. Gietter, R. C. Pupillo, G. P. A. Yap, T. P. Beebe, J. Rosenthal and D. A. Watson, *Chem. Sci.*, 2012, **4**, 437–443.

68 E. R. Young, J. Rosenthal and D. G. Nocera, *Chem. Sci.*, 2012, **3**, 455–459.

69 A. M. Potocny, A. J. Pistner, G. P. A. Yap and J. Rosenthal, *Inorg. Chem.*, 2017, **56**, 12703–12711.